

TU-TP/98-01
January, 1998

Analysis of neutrino oscillation in three-flavor neutrinos

T. Teshima*, T. Sakai and O. Inagaki

Department of Applied Physics, Chubu University, Kasugai 487, Japan

Abstract

We analyzed the solar, terrestrial and atmospheric neutrinos experiments using the three-flavor neutrino framework and got the allowed regions for parameters (Δm_{12}^2 , $\sin^2 2\theta_{12}$, Δm_{23}^2 , θ_{13} , θ_{23}). In solar neutrino experiments, we got the large angle solution (Δm_{12}^2 , $\sin^2 2\theta_{12}$) = ($4 \times 10^{-6} - 7 \times 10^{-5}$ eV 2 , 0.6–0.9) and small angle solution ($3 \times 10^{-6} - 1.2 \times 10^{-5}$ eV 2 , 0.003–0.01) for $\theta_{13} = 0^\circ - 20^\circ$. From the terrestrial and atmospheric neutrino experiments, we got the allowed regions ($\theta_{13} < 4^\circ$, $24^\circ < \theta_{23} < 26^\circ$) for $\Delta m_{23}^2 = 2$ eV 2 , ($\theta_{13} < 4^\circ$, $24^\circ < \theta_{23} < 45^\circ$) for $\Delta m_{23}^2 = 0.2$ eV 2 and ($\theta_{13} < 14^\circ$, $\theta_{23} \sim 40^\circ$) for $\Delta m_{23}^2 = 0.02$ eV 2 . It seems that the large angle solution for (Δm_{12}^2 , $\sin^2 2\theta_{12}$) is favored than the small angle solution from the analysis of zenith angle dependence in atmospheric neutrino sub-GeV experiment.

I. INTRODUCTION

The problem of neutrino masses and oscillations is one of the most interesting issues to study physics beyond the standard model (SM) [1]. In many experiments which are under way, indications in favor of neutrino masses and oscillations have been obtained. In these experiments, the solar neutrino experiments [2–5] measure the event rates significantly

lower than the ones predicted by the standard solar model, and the atmospheric neutrino experiments [6–8] observe an anomaly referred to as the unexpected difference between the measured and predicted μ -like and e -like neutrinos. Another indication in favor of non-zero neutrino masses is in the cosmological analysis by dark matter [9].

On the other hand, terrestrial neutrino experiments searching for the neutrino masses and oscillations are under way. The E531 [10], CHORUS and NOMAD [11] experiments using the beam from accelerator search for ν_τ appearance in a ν_μ , and E776 [12], KARMEN [13] and LSND [14] experiments using the accelerator beams are searching for $\nu_\mu \rightarrow \nu_e$ and $\bar{\nu}_\mu \rightarrow \bar{\nu}_e$ oscillations. The experiments using nuclear power reactor [15] search for the disappearance of $\bar{\nu}_e$, in which $\bar{\nu}_e \rightarrow \bar{\nu}_X$ ($X = \mu, \tau$) transitions are expected. These experiments do not observe significantly large neutrino transitions.

In this paper, we analyze the data of current solar, terrestrial and atmospheric experiments in a framework where the three neutrinos have masses and mix each other, and search the allowed regions of parameters (Δm_{12}^2 , $\sin^2 2\theta_{12}$, Δm_{23}^2 , θ_{13} , θ_{23}) characterizing the masses and mixing of three-flavor neutrinos. Although there are many analyses which study the solar, atmospheric and terrestrial neutrino problems in three-flavor neutrinos framework [16–18], we study more thoroughly these problems including the analysis of zenith angle dependence in recent SuperKamiokande atmospheric experiment [19,20]. After the analyses of experiments for neutrino oscillation, we will present a matrix of neutrino mixing ascribed from the allowed regions of parameters obtained.

II. NEUTRINO OSCILLATION

Weak currents for the interactions producing and absorbing neutrinos are described as

$$J_\mu = 2 \sum_{\alpha, \beta=1}^3 \bar{l}_{L\alpha} \gamma_\mu U_{l\alpha\beta} \nu_{L\beta}, \quad (1)$$

where l_α ($l_1 = e$, $l_2 = \mu$, $l_3 = \tau$) represents the lepton flavor, ν_β the neutrino mass eigenstate and U is the lepton mixing matrix. U is the unitary matrix corresponding to the CKM matrix V_{CKM}^\dagger for quarks defined by

$$U = U_l U_\nu^\dagger, \quad (2)$$

where the unitary matrices U_l and U_ν transform mass matrices M_l for charged leptons and M_ν for neutrinos to diagonal mass matrices as

$$\begin{aligned} U_l M^l U_l^{-1} &= \text{diag}[m_e, m_\mu, m_\tau], \\ U_\nu M^\nu U_\nu^{-1} &= \text{diag}[m_1, m_2, m_3]. \end{aligned} \quad (3)$$

We present the unitary matrix neglecting the CP violation phases as

$$\begin{aligned}
U &= e^{i\theta_{23}\lambda_7} e^{i\theta_{13}\lambda_5} e^{i\theta_{12}\lambda_2} \\
&= \begin{pmatrix} c_{12}^\nu c_{13}^\nu & s_{12}^\nu c_{13}^\nu & s_{13}^\nu \\ -s_{12}^\nu c_{23}^\nu - c_{12}^\nu s_{23}^\nu s_{13}^\nu & c_{12}^\nu c_{23}^\nu - s_{12}^\nu s_{23}^\nu s_{13}^\nu & s_{23}^\nu c_{13}^\nu \\ s_{12}^\nu s_{23}^\nu - c_{12}^\nu c_{23}^\nu s_{13}^\nu & -c_{12}^\nu s_{23}^\nu - s_{12}^\nu c_{23}^\nu s_{13}^\nu & c_{23}^\nu c_{13}^\nu \end{pmatrix}, \\
&\quad c_{ij}^\nu = \cos \theta_{ij}^\nu, \quad s_{ij}^\nu = \sin \theta_{ij}^\nu,
\end{aligned} \tag{4}$$

where λ_i 's are Gell-Mann matrices.

The probabilities for transitions $\nu_{l_\alpha} \rightarrow \nu_{l_\beta}$ are written as

$$\begin{aligned}
P(\nu_{l_\alpha} \rightarrow \nu_{l_\beta}) &= |<\nu_{l_\beta}(t)|\nu_{l_\alpha}(0)>|^2 = \delta_{l_\alpha l_\beta} + p_{\nu_{l_\alpha} \rightarrow \nu_{l_\beta}}^{12} S_{12} + p_{\nu_{l_\alpha} \rightarrow \nu_{l_\beta}}^{23} S_{23} + p_{\nu_{l_\alpha} \rightarrow \nu_{l_\beta}}^{31} S_{31}, \\
p_{\nu_{l_\alpha} \rightarrow \nu_{l_\beta}}^{12} &= -2\delta_{l_\alpha l_\beta}(1 - 2U_{l_\alpha 3}^2) + 2(U_{l_\alpha 1}^2 U_{l_\beta 1}^2 + U_{l_\alpha 2}^2 U_{l_\beta 2}^2 - U_{l_\alpha 3}^2 U_{l_\beta 3}^2), \\
p_{\nu_{l_\alpha} \rightarrow \nu_{l_\beta}}^{23} &= -2\delta_{l_\alpha l_\beta}(1 - 2U_{l_\alpha 1}^2) + 2(-U_{l_\alpha 1}^2 U_{l_\beta 1}^2 + U_{l_\alpha 2}^2 U_{l_\beta 2}^2 + U_{l_\alpha 3}^2 U_{l_\beta 3}^2), \\
p_{\nu_{l_\alpha} \rightarrow \nu_{l_\beta}}^{31} &= -2\delta_{l_\alpha l_\beta}(1 - 2U_{l_\alpha 2}^2) + 2(U_{l_\alpha 1}^2 U_{l_\beta 1}^2 - U_{l_\alpha 2}^2 U_{l_\beta 2}^2 + U_{l_\alpha 3}^2 U_{l_\beta 3}^2),
\end{aligned} \tag{5}$$

where S_{ij} is the term representing the neutrino oscillation;

$$S_{ij} = \sin^2 1.27 \frac{\Delta m_{ij}^2}{E} L, \tag{6}$$

in which $\Delta m_{ij}^2 = |m_i^2 - m_j^2|$, E and L are measured in units eV², MeV and m, respectively. From the unitarity of U , we get relations

$$p_{\nu_{l_\alpha} \rightarrow \nu_e}^{ij} + p_{\nu_{l_\alpha} \rightarrow \nu_\mu}^{ij} + p_{\nu_{l_\alpha} \rightarrow \nu_\tau}^{ij} = 0, \quad i, j = 1, 2, 3, \quad l_\alpha = e, \mu, \tau. \tag{7}$$

The values of neutrino masses are not known precisely, but we know that if one identifies the dark matter of universe (or at least its hot dark matter component) with neutrino matter one has [9]

$$m_1 + m_2 + m_3 \sim \text{several eV}. \tag{8}$$

We do not use this value strictly in present analysis, but we consider that the sum of neutrino masses is not so small. In two-flavor neutrinos analyses in which one mass parameter Δm^2 appears for solar neutrino experiments, the result that Δm^2 is $10^{-4} - 10^{-5}$ eV² or $\sim 10^{-10}$ eV² is obtained [21]. For atmospheric experiments, Δm^2 is obtained as $10^{-1} - 10^{-2}$ eV² [21]. Then it seems that two neutrinos masses in three neutrinos are very close and another one is rather far away from them. Then we assume that three neutrino masses have such a mass hierarchy as

$$m_1 \approx m_2 \ll m_3. \tag{9}$$

In the the mass hierarchy Eq. (9), $\Delta m_{12}^2 \ll \Delta m_{23}^2 \simeq \Delta m_{13}^2$, the expression Eq. (5) for the transition probabilities $P(\nu_{l_\alpha} \rightarrow \nu_{l_\beta})$ are rewritten as

$$\begin{aligned}
P(\nu_e \rightarrow \nu_e) &= 1 - 2(1 - 2U_{e3}^2 - U_{e1}^4 - U_{e2}^4 + U_{e3}^4)S_{12} - 4U_{e3}^2(1 - U_{e3}^2)S_{23}, \\
P(\nu_\mu \rightarrow \nu_\mu) &= 1 - 2(1 - 2U_{\mu3}^2 - U_{\mu1}^4 - U_{\mu2}^4 + U_{\mu3}^4)S_{12} - 4U_{\mu3}^2(1 - U_{\mu3}^2)S_{23}, \\
P(\nu_\tau \rightarrow \nu_\tau) &= 1 - 2(1 - 2U_{\tau3}^2 - U_{\tau1}^4 - U_{\tau2}^4 + U_{\tau3}^4)S_{12} - 4U_{\tau3}^2(1 - U_{\tau3}^2)S_{23}, \\
P(\nu_\mu \rightarrow \nu_e) &= P(\nu_e \rightarrow \nu_\mu) = 2(U_{\mu1}^2 U_{e1}^2 + U_{\mu2}^2 U_{e2}^2 - U_{\mu3}^2 U_{e3}^2)S_{12} + 4U_{e3}^2 U_{\mu3}^2 S_{23}, \\
P(\nu_\tau \rightarrow \nu_e) &= P(\nu_e \rightarrow \nu_\tau) = 2(U_{\tau1}^2 U_{e1}^2 + U_{\tau2}^2 U_{e2}^2 - U_{\tau3}^2 U_{e3}^2)S_{12} + 4U_{e3}^2 U_{\tau3}^2 S_{23}, \\
P(\nu_\tau \rightarrow \nu_\mu) &= P(\nu_\mu \rightarrow \nu_\tau) = 2(U_{\tau1}^2 U_{\mu1}^2 + U_{\tau2}^2 U_{\mu2}^2 - U_{\tau3}^2 U_{\mu3}^2)S_{12} + 4U_{\mu3}^2 U_{\tau3}^2 S_{23}.
\end{aligned} \tag{10}$$

III. NUMERICAL ANALYSES OF NEUTRINO OSCILLATION IN THREE-FLAVOR NEUTRINOS

A. Solar neutrinos

We first analyze the solar neutrino experiments. Considering the matter effects (MSW effect [22]) in three-flavor neutrinos, the transition probability for $\nu_e \rightarrow \nu_e$ is expressed as [17]

$$P_{3\nu}^{\text{MSW}}(\Delta m_{12}^2, \theta_{12}, \theta_{13}, E) = \cos^4 \theta_{13} P_{2\nu}^{\text{MSW}}(\Delta m_{12}^2, \theta_{12}, \theta_{13}, E) + \sin^4 \theta_{13} C \tag{11a}$$

$$\begin{aligned}
P_{2\nu}^{\text{MSW}}(\Delta m_{12}^2, \theta_{12}, \theta_{13}, E) &= \frac{1}{2} + \left(\frac{1}{2} - \Theta(A \cos^2 \theta_{13} - \Delta m_{12}^2 \cos 2\theta_{12}) P_c(\theta_{12}, E) \right) \\
&\quad \times \cos 2\theta_{12} \cos 2\theta_{12}^m,
\end{aligned} \tag{11b}$$

$$P_c(\theta_{12}, E) = \exp\left(-\frac{\pi}{2}\gamma(\theta_{12}, E)\right), \tag{11c}$$

$$\gamma(\theta_{12}, E) = \frac{\Delta m_{12}^2 \sin^2 2\theta_{12}}{2E \cos 2\theta_{12} |dN_e/N_e dx|_0}, \tag{11d}$$

where Θ is the theta function, $A = 2\sqrt{2}G_F N_e E$ (G_F is Fermi constant, N_e number of electron per cm^3 at the production point of neutrinos in the sun and E the energy of neutrino), P_c the Landau-Zener-Stueckerberg crossing probability, γ is the adiabaticity parameter ($|\cdot\cdot\cdot|_0$ represents the value at the production point of neutrinos) and θ_{12}^m the mixing angle at the production point. $P_{2\nu}^{\text{MSW}}$ is the transition probability with a replacement of $N_e \rightarrow N_e \cos 2\theta_{13}$ in two-flavor neutrinos transition probability. This expression is obtained from an approximation;

$$\Theta[A - (m_3^2 - \Lambda/2) \cos 2\theta_{13}] \exp\left(-\frac{\pi}{4} \frac{(m_3^2 - \Lambda/2)}{|dN_e/N_e dx|_0 E} \frac{\sin^2 2\theta_{13}}{\cos 2\theta_{13}}\right) \ll 1, \tag{12}$$

where $\Lambda = ((m_1^2 + m_2^2) - (m_2^2 - m_1^2) \cos 2\theta_{12})$. This approximation is reasonable for present assumption of mass hierarchy Eq. (9) because of $A \ll m_3^2 - \Lambda/2$ and $m_3^2 - \Lambda/2 \gg |dN_e/N_e dx|_0 E$.

The ratios of the detected e neutrino fluxes to the expected e neutrino fluxes deduced from the standard solar model (SSM) [23] are expressed by using the transition probability $P_{3\nu}^{\text{MSW}}$ as

$$R = \frac{\int_{E_{\min}}^{E_{\max}} P_{3\nu}^{\text{MSW}}(E) f(E) dE}{\int_{E_{\min}}^{E_{\max}} f(E) dE}, \quad (13)$$

where $f(E)$ is the product of the spectral function of neutrino flux and detector sensitivity. The neutrino flux is the sum of many neutrino fluxes produced by the various nuclear fusion reaction at the center of the sun. The detector sensitivity also depends to the neutrino energy. Numerical results for neutrino flux and detector sensitivity are analyzed precisely in Ref. [23]. For $f(E)$ used in this paper, see Appendix A.

In our analysis, we use the following three experimental data for R :

Ga experiment [2,3]:

$$R = 0.534 \pm 0.087, \quad (14a)$$

Cl experiment [4]:

$$R = 0.274 \pm 0.046, \quad (14b)$$

water Cherenkov experiment [5]:

$$R = 0.437 \pm 0.092. \quad (14c)$$

In Ga experiment, we combined the SAGE [2] and GALLEX [3] data. First we estimate the numerical values R for $\theta_{13} = 0$ which corresponds to two-flavor neutrinos case using the Eq. (13), and show the contours of R on $\sin^2 2\theta_{12} - \Delta m_{12}^2$ plane in Fig. 1. Each contour denoted as Ga, Cl and Kam corresponds to the upper and lower values of R in Eq. (14) for Ga, Cl and Kamiokande's water Cherenkov experiment. There are two solutions which are denoted as common areas enclosed by each two contours of Ga, Cl and Kam. These are called as large solution and small solution. This result is similar to the one obtained in various analyses [24].

Next we estimate the numerical values R for the case of $\theta_{13} \neq 0$. In Fig. 2, we show the allowed regions of the combined Ga, Cl and Kam experiments using the χ -square, where the solid thin, solid thick and dotted lines define the regions allowed at 99% ($\chi^2 = 9.2$), 95% ($\chi^2 = 6.0$) and 90% ($\chi^2 = 4.5$) C.L., respectively. Fig. 2(a) - Fig. 2(h) show the allowed regions for $\theta_{13} = 0^\circ - 50^\circ$. Fig. 2(a) shows the $\theta_{13} = 0$ case, thus this shows the two-flavor neutrinos' solution. These results are similar to the ones obtained by Ref. [18]. Numerically, we show the allowed regions in 95% C.L.;

for $\theta_{13} = 0^\circ - 20^\circ$

$$\left. \begin{aligned} \Delta m_{12}^2 &= 4 \times 10^{-6} - 7 \times 10^{-5} \text{ eV}^2 \\ \sin^2 2\theta_{12} &= 0.6 - 0.9 \end{aligned} \right\} \text{large angle solution} \quad (15a)$$

$$\left. \begin{array}{l} \Delta m_{12}^2 = 3 \times 10^{-6} - 1.2 \times 10^{-5} \text{eV}^2 \\ \sin^2 2\theta_{12} = 0.003 - 0.01 \end{array} \right\} \text{small angle solution} \quad (15b)$$

for $\theta_{13} = 25^\circ - 40^\circ$

$$\left. \begin{array}{l} \Delta m_{12}^2 = 2 \times 10^{-6} - 3 \times 10^{-5} \text{eV}^2 \\ \sin^2 2\theta_{12} = 0.001 - 0.01 \end{array} \right\} \text{small angle solution} \quad (15c)$$

for $\theta_{13} = 45^\circ - 50^\circ$

$$\left. \begin{array}{l} \Delta m_{12}^2 = 2 \times 10^{-6} - 3 \times 10^{-5} \text{eV}^2 \\ \sin^2 2\theta_{12} = 0.001 - 0.7 \end{array} \right\} \quad (15d)$$

The characteristic feature of three-flavor neutrinos' solution is as follows; increasing θ_{13} from 0° to 25° , the small mixing solution and the large mixing solution merge in a single solution, further increasing θ_{13} to 50° , the allowed region becomes broader and next shrinks and lastly disappears.

B. Terrestrial neutrinos

In terrestrial experiments, there are two types of experiment: short baseline and long baseline experiment. In present study, we analyze the short baseline experiment. In the short baseline experiments, there are E531 [10], CHORUS and NOMAD [11] accelerator experiments searching for ν_τ appearance in ν_μ . We use the data of E531, CHORUS and NOMAD experiments;

$$\begin{aligned} P(\nu_\mu \rightarrow \nu_\tau) &< 2 \times 10^{-3} \quad (90\% \text{ C.L.}), \\ L/E &\sim 0.02. \end{aligned} \quad (16)$$

For the experiments searching for $\nu_\mu \rightarrow \nu_e$ and $\bar{\nu}_\mu \rightarrow \bar{\nu}_e$ oscillations, there are E776 [12], KARMEN [13] and LSND [14] accelerator experiments;

$$\begin{aligned} P(\nu_\mu \rightarrow \nu_e) &< 3 \times 10^{-3} \quad (90\% \text{ C.L.}), \quad \text{E776} \\ L &= 1\text{km}, \quad E \sim 1\text{GeV}, \end{aligned} \quad (17a)$$

$$\begin{aligned} P(\bar{\nu}_\mu \rightarrow \bar{\nu}_e) &< 3.1 \times 10^{-3} \quad (90\% \text{ C.L.}), \quad \text{KARMEN} \\ L &= 17.5\text{m}, \quad E < 50\text{MeV}, \end{aligned} \quad (17b)$$

$$\begin{aligned} P(\bar{\nu}_\mu \rightarrow \bar{\nu}_e) &= 3.4^{+2.0}_{-1.8} \pm 0.7 \times 10^{-3}, \quad \text{LSND} \\ L &= 30\text{m}, \quad E \sim 36 - 60\text{MeV}. \end{aligned} \quad (17c)$$

Furthermore, we analyse the experiments using nuclear power reactor [15] searching for the disappearance of $\bar{\nu}_e$,

$$1 - P(\bar{\nu}_e \rightarrow \bar{\nu}_e) < 10^{-2} \quad (90\% \text{ C.L.}), \quad (18)$$

$$L = 15, 40, 95\text{m}, \quad E \sim 1 - 6\text{MeV}.$$

In the short baseline experiments, the neutrino propagation length L is about $L \lesssim 1\text{km}$, then $S_{12} = \sin^2 1.27 \frac{\Delta m_{12}^2}{E} L$ is very small because $\Delta m_{12}^2 \sim 10^{-5} - 10^{-4}\text{eV}^2$ suggested from last solar neutrino analyses. Then, the S_{23} term is dominant in the transition probability Eq. (10). Seeing that the mixing parts proportional to S_{23} are $4U_{e3}^2(1-U_{e3}^2)$, $4U_{\mu 3}^2(1-U_{\mu 3}^2)$ and $4U_{\tau 3}^2(1-U_{\tau 3}^2)$, the transition probabilities in present short baseline terrestrial experiments seem to be insensitive to the parameters; Δm_{12}^2 and θ_{12} .

We show the contour plots of the allowed regions on $(\tan^2 \theta_{13}, \tan^2 \theta_{23})$ plane determined by the probability P expressed in Eq. (10) and above experimental data Eqs. (16), (17) and (18) in Fig. 3. Allowed regions are corners, left and right hand sides surrounded by curves. Curves represent the boundary of 90 % C.L. of P . We fixed the parameters Δm_{12}^2 and θ_{12} as $\Delta m_{12}^2 = 10^{-5}\text{eV}^2$ and $\sin^2 2\theta_{12} = 0.8$, and the parameter Δm_{13}^2 to be various values from 0.02eV^2 to 20eV^2 . Although we fix the parameters Δm_{12}^2 and θ_{12} as $\Delta m_{12}^2 = 10^{-5}\text{eV}^2$ and $\sin^2 2\theta_{12} = 0.01$, the results are not changed. Dotted lines show the allowed regions restricted by the LSND data. From these results, we see that the numerical allowed regions on $(\theta_{13}, \theta_{23})$ without the LSND data are as follows;

$$\text{for } \Delta m_{23}^2 = 20\text{eV}^2$$

$$(< 4^\circ, < 2^\circ), \quad (< 2^\circ, > 88^\circ), \quad (> 86^\circ - 88^\circ, \text{ any}), \quad (19a)$$

$$\text{for } \Delta m_{23}^2 = 2\text{eV}^2$$

$$(< 4^\circ, < 26^\circ), \quad (< 2^\circ, > 65^\circ), \quad (> 86^\circ - 88^\circ, \text{ any}), \quad (19b)$$

$$\text{for } \Delta m_{23}^2 = 0.2\text{eV}^2$$

$$(< 4^\circ, \text{ any}), \quad (> 86^\circ, \text{ any}), \quad (19c)$$

$$\text{for } \Delta m_{23}^2 = 0.02\text{eV}^2$$

$$(< 12^\circ, \text{ any}), \quad (> 78^\circ, \text{ any}) \quad (19d)$$

$$\text{for } \Delta m_{23}^2 < 0.005\text{eV}^2$$

$$\text{all regions are allowed.} \quad (19e)$$

If we combine the LSND data with the above analyses, the allowed region disappears lower than 0.2eV^2 of the Δm_{23}^2 value. Furthermore, combining the solar neutrino solutions with this terrestrial ones, the allowed regions larger than 50° of θ_{13} on terrestrial neutrino are excluded.

C. Atmospheric neutrinos

The evidence for an anomaly in atmospheric neutrino experiments was pointed out by the Kamiokande Collaboration [6,7] and IMB Collaboration [8] using the water-Cherenkov

experiments. More recently, SuperKamiokande Collaboration [19,20] reports the more precise results on anomaly in atmospheric neutrino. We tabulate these results in Table II. That the double ratio, $R(\mu/e) \equiv R_{\text{expt}}(\mu/e)/R_{\text{MC}}(\mu/e)$, is less than 1 is the atmospheric neutrino's anomaly. In Table II, sub-GeV experiments detect the visible-energy less than 1.33GeV, and in the second column (total exposure), left number represents the detector exposure in which fully contained events are detected and right numbers partially contained events.

The ratios $R_{\text{expt}}(\mu/e)$ and $R_{\text{MC}}(\mu/e)$ are defined as

$$R_{\text{expt}}(\mu/e) = \frac{\sum_{\alpha} \int \epsilon_{\mu}(E_{\mu}) \sigma_{\mu}(E_{\alpha}, E_{\mu}) F_{\alpha}(E_{\alpha}, \theta_{\alpha}) P(\nu_{\alpha} \rightarrow \nu_{\mu}) dE_{\mu} dE_{\alpha} d\theta_{\alpha}}{\sum_{\alpha} \int \epsilon_{e}(E_{e}) \sigma_{e}(E_{\alpha}, E_{e}) F_{\alpha}(E_{\alpha}, \theta_{\alpha}) P(\nu_{\alpha} \rightarrow \nu_{e}) dE_{e} dE_{\alpha} d\theta_{\alpha}}, \quad (20a)$$

$$R_{\text{MC}}(\mu/e) = \frac{\sum_{\alpha} \int \epsilon_{\mu}(E_{\mu}) \sigma_{\mu}(E_{\alpha}, E_{\mu}) F_{\alpha}(E_{\alpha}, \theta_{\alpha}) dE_{\mu} dE_{\alpha} d\theta_{\alpha}}{\sum_{\alpha} \int \epsilon_{e}(E_{e}) \sigma_{e}(E_{\alpha}, E_{e}) F_{\alpha}(E_{\alpha}, \theta_{\alpha}) dE_{e} dE_{\alpha} d\theta_{\alpha}}, \quad (20b)$$

where the summation \sum_{α} are taken in μ , e neutrino and μ , e antineutrino. $\epsilon_{\beta}(E_{\beta})$ is the detection efficiency of the detector for β -type charged lepton with energy E_{β} , σ_{β} is the differential cross section of ν_{β} and $F_{\alpha}(E_{\alpha}, \theta_{\alpha})$ is the incident ν_{α} flux with energy E_{α} and zenith angle θ_{α} . $P(\nu_{\alpha} \rightarrow \nu_{\beta})$ is the transition probability Eq. (10) and it depends on the energy E_{α} and the distance L which depends on zenith angle θ_{α} as $L = \sqrt{(r+h)^2 - r^2 \sin^2 \theta_{\alpha}} - r \cos \theta_{\alpha}$, where r is the radius of the Earth and h is the altitude of production point of atmospheric neutrino.

Although informations of $F_{\alpha}(E_{\alpha}, \theta_{\alpha})$ etc. are given in Refs. [25–27], we use the MC predictions for $f_{\alpha}(E_{\alpha}, \theta_{\alpha}) \equiv \sum_{\alpha} \int \epsilon_{\mu}(E_{\mu}) \sigma_{\mu}(E_{\alpha}, E_{\mu}) F_{\alpha}(E_{\alpha}, \theta_{\alpha}) dE_{\mu}$ in Ref. [6] for sub-GeV experiment and Ref. [7] for multi-GeV experiment. Explicit E_{α} dependence of $f_{\alpha}(E_{\alpha}, \theta_{\alpha})$ are shown in Appendix B. Since $P(\nu_{\alpha} \rightarrow \nu_{\mu})$ and $P(\nu_{\alpha} \rightarrow \nu_{e})$ are the functions of $(\Delta m_{12}^2, \Delta m_{23}^2, \theta_{12}, \theta_{23}, L, E)$, the double ratio $R(\mu/e)$ which is integrated in neutrino energy E and zenith angle θ (related to L) is the function of $(\Delta m_{12}^2, \Delta m_{23}^2, \theta_{12}, \theta_{13}, \theta_{23})$. We estimate the $R(\mu/e)$ fixing the parameters $(\delta m_{12}^2, \sin^2 2\theta)$ on the allowed values Eq. (15) predicted by the solar neutrino experiments; $\delta m_{12}^2 = 3 \times 10^{-5} \text{eV}^2$, $\sin^2 2\theta_{12} = 0.7$ which corresponds to large angle solution and $\delta m_{12}^2 = 10^{-5} \text{eV}^2$, $\sin^2 2\theta_{12} = 0.005$ which corresponds to small angle solution.

In Fig. 4, we showed the contour plots of double ratio $R(\mu/e)$ on $\tan^2 \theta_{13} - \tan^2 \theta_{23}$ plane for various Δm_{23}^2 . Contour lines correspond the upper and lower values of $R(\mu/e)$ in Table II. We showed the plots of sub-GeV experiment in Fig. 4(a)-(d) and plots of multi-GeV one in Fig. 4(e)-(h), and in these figures solid lines denote the large angle solution plots and dotted lines the small angle solution plots. In Fig. (a)-(c), the allowed regions are surrounded by two solid lines (or dotted lines) and in Fig. (d), by two outer lines (or dotted lines) and inner solid line (or dotted line). In Fig. (e)-(h), dotted lines are close in solid lines. In Fig. (e)-(g), allowed regions are surrounded by two outer solid lines (or dotted lines) and inner solid line (or dotted line) and in Fig. (h), by two solid lines (or dotted lines).

Observing the allowed regions obtained terrestrial neutrino experiments Fig. 3 and the present allowed regions obtained atmospheric neutrino experiments, we obtain the allowed

regions satisfying all experiments. First, we show the allowed regions of $(\theta_{13}, \theta_{23})$ for the large angle solution and small angle solution in sub-GeV experiment:

| | large angle solution | small angle solution |
|--|--|--|
| for $\Delta m_{23}^2 = 20\text{eV}^2$ | no allowed region | no allowed region |
| for $\Delta m_{23}^2 = 2\text{eV}^2$ | $(\theta_{13} < 4^\circ, 18^\circ < \theta_{23} < 26^\circ)$ | $\begin{cases} (\theta_{13} < 4^\circ, 24^\circ < \theta_{23} < 26^\circ) \\ (\theta_{13} < 2^\circ, 64^\circ < \theta_{23} < 66^\circ) \end{cases}$ |
| for $\Delta m_{23}^2 = 0.2\text{eV}^2$ | $(\theta_{13} < 4^\circ, 18^\circ < \theta_{23} < 62^\circ)$ | $(\theta_{13} < 4^\circ, 24^\circ < \theta_{23} < 66^\circ)$ |
| for $\Delta m_{23}^2 = 0.02\text{eV}^2$ | $\begin{cases} (\theta_{13} < 12^\circ, 17^\circ < \theta_{23} < 38^\circ) \\ (\theta_{13} < 12^\circ, 47^\circ < \theta_{23} < 63^\circ) \end{cases}$ | $\begin{cases} (\theta_{13} < 14^\circ, 23^\circ < \theta_{23} < 41^\circ) \\ (\theta_{13} < 14^\circ, 49^\circ < \theta_{23} < 67^\circ) \end{cases}$ |
| for $\Delta m_{23}^2 = 0.002\text{eV}^2$ | $\begin{cases} (\theta_{13} < 29^\circ, 27^\circ < \theta_{23} < 52^\circ) \\ (39^\circ < \theta_{13} < 59^\circ, 76^\circ < \theta_{23}) \end{cases}$ | $\begin{cases} (\theta_{13} < 34^\circ, 34^\circ < \theta_{23} < 56^\circ) \\ (34^\circ < \theta_{13} < 56^\circ, 56^\circ < \theta_{23}) \end{cases}$ |

second, in multi-GeV experiment:

| | large angle solution | small angle solution |
|--|--|--|
| for $\Delta m_{23}^2 = 20\text{eV}^2$ | no allowed region | no allowed region |
| for $\Delta m_{23}^2 = 2\text{eV}^2$ | $\begin{cases} (\theta_{13} < 4^\circ, 24^\circ < \theta_{23} < 26^\circ) \\ (\theta_{13} < 2^\circ, 64^\circ < \theta_{23} < 66^\circ) \end{cases}$ | $\begin{cases} (\theta_{13} < 4^\circ, 24^\circ < \theta_{23} < 26^\circ) \\ (\theta_{13} < 2^\circ, 64^\circ < \theta_{23} < 66^\circ) \end{cases}$ |
| for $\Delta m_{23}^2 = 0.2\text{eV}^2$ | $(\theta_{13} < 4^\circ, 24^\circ < \theta_{23} < 66^\circ)$ | $(\theta_{13} < 4^\circ, 24^\circ < \theta_{23} < 66^\circ)$ |
| for $\Delta m_{23}^2 = 0.02\text{eV}^2$ | $(\theta_{13} < 12^\circ, 41^\circ < \theta_{23} < 49^\circ)$ | $(\theta_{13} < 12^\circ, 41^\circ < \theta_{23} < 49^\circ)$ |
| for $\Delta m_{23}^2 = 0.002\text{eV}^2$ | $(22^\circ < \theta_{13} < 68^\circ, 45^\circ < \theta_{23})$ | $(22^\circ < \theta_{13} < 68^\circ, 45^\circ < \theta_{23})$ |

If we combine the LSND experiment with above terrestrial data, allowed regions are restricted as follows,

sub-GeV case:

| | large angle solution | small angle solution |
|--|--|--|
| for $\Delta m_{23}^2 = 2\text{eV}^2$ | $(2^\circ < \theta_{13} < 4^\circ, 18^\circ < \theta_{23} < 26^\circ)$ | $\begin{cases} (2^\circ < \theta_{13} < 4^\circ, 24^\circ < \theta_{23} < 26^\circ) \\ (0.8^\circ < \theta_{13} < 2^\circ, 64^\circ < \theta_{23} < 66^\circ) \end{cases}$ |
| for $\Delta m_{23}^2 = 0.2\text{eV}^2$ | no allowed region | no allowed region |

multi-GeV case:

| | large angle solution | small angle solution |
|--|--|--|
| for $\Delta m_{23}^2 = 2\text{eV}^2$ | $\begin{cases} (2^\circ < \theta_{13} < 4^\circ, \\ \quad 24^\circ < \theta_{23} < 26^\circ) \\ (0.8^\circ < \theta_{13} < 2^\circ, \\ \quad 64^\circ < \theta_{23} < 66^\circ) \end{cases}$ | $\begin{cases} (2^\circ < \theta_{13} < 4^\circ, \\ \quad 24^\circ < \theta_{23} < 26^\circ) \\ (0.8^\circ < \theta_{13} < 2^\circ, \\ \quad 64^\circ < \theta_{23} < 66^\circ) \end{cases}$ |
| for $\Delta m_{23}^2 = 0.2\text{eV}^2$ | no allowed region | no allowed region |

(24a)
(24b)

Although there are allowed regions satisfying both terrestrial and atmospheric experimental restrictions, all of these solutions do not satisfy the zenith angle dependence of $R(\mu/e)$ for atmospheric neutrino experiments. From resent SuperKamiokande experiments [19,20], zenith angle dependence seems to be more definite than that obtained previously [6,7]: the double ratio $R(\mu/e)$ for sub-GeV experiment seems to decrease monotonically as zenith angle θ increases from $\theta = 0^\circ$ to $\theta = 180^\circ$ and $R(\mu/e)$ for multi-GeV experiments seems to decrease as zenith angle θ increases from $\theta = 0^\circ$ to $\theta = 180^\circ$. Among the allowed solutions obtained above, Eqs. (21) and (22) (or (23) and (24)), the large angle ($\sin^2 2\theta_{12} \sim 0.7$) solutions with $\theta_{23} < 45^\circ$ satisfy the monotonic decreasing of the $R(\mu/e)$ in sub-GeV neutrino experiment. This solution also decreases in multi-GeV experiment as zenith angle increases.

In Fig. 5(a), we showed the zenith angle ($\cos \theta$) dependence of $R(\mu/e)$ in sub-GeV experiment on the typical parameters for large angle solution ($\Delta m_{12}^2 = 3 \times 10^{-5}\text{eV}^2$, $\sin^2 2\theta_{12} = 0.7$, $\Delta m_{23}^2 = 0.2\text{eV}^2$, $\theta_{13} = 4^\circ$, $\theta_{23} = 25^\circ$) by solid curve and small angle solution ($\Delta m_{12}^2 = 10^{-5}\text{eV}^2$, $\sin^2 2\theta_{12} = 0.007$, $\Delta m_{23}^2 = 0.2\text{eV}^2$, $\theta_{13} = 4^\circ$, $\theta_{23} = 25^\circ$) by dotted curve. Experimental data is referred to SuperKamiokande [20]. Fig. 5(b) represents the zenith angle ($\cos \theta$) dependence of $R(\mu/e)$ in multi-GeV experiment on the parameters for large angle solution ($\Delta m_{12}^2 = 3 \times 10^{-5}\text{eV}^2$, $\sin^2 2\theta_{12} = 0.7$, $\Delta m_{23}^2 = 0.2\text{eV}^2$, $\theta_{13} = 4^\circ$, $\theta_{23} = 30^\circ$) (solid curve) and small angle solution ($\Delta m_{12}^2 = 10^{-5}\text{eV}^2$, $\sin^2 2\theta_{12} = 0.007$, $\Delta m_{23}^2 = 0.2\text{eV}^2$, $\theta_{13} = 4^\circ$, $\theta_{23} = 30^\circ$) (dotted curve).

We summarize the solution satisfying the solar, terrestrial and atmospheric experiments as follows;

| | |
|---|-------|
| for $\Delta m_{23}^2 = 2\text{eV}^2$ | |
| $\begin{cases} \Delta m_{12}^2 = 4 \times 10^{-6} - 7 \times 10^{-5}\text{eV}^2, \quad \sin^2 2\theta_{12} = 0.6 - 0.9, \\ \theta_{13} < 4^\circ, \quad 24^\circ < \theta_{23} < 26^\circ, \end{cases}$ | (25a) |

| | |
|---|-------|
| for $\Delta m_{23}^2 = 0.2\text{eV}^2$ | |
| $\begin{cases} \Delta m_{12}^2 = 4 \times 10^{-6} - 7 \times 10^{-5}\text{eV}^2, \quad \sin^2 2\theta_{12} = 0.6 - 0.9, \\ \theta_{13} < 4^\circ, \quad 24^\circ < \theta_{23} < 45^\circ. \end{cases}$ | (25b) |

| | |
|---|--|
| for $\Delta m_{23}^2 = 0.02\text{eV}^2$ | |
|---|--|

$$\begin{cases} \Delta m_{12}^2 = 4 \times 10^{-6} - 7 \times 10^{-5} \text{eV}^2, \sin^2 2\theta_{12} = 0.6 - 0.9, \\ \theta_{13} < 12^\circ, \theta_{23} \sim 40^\circ. \end{cases} \quad (25c)$$

If we include the LSND experiment in terrestrial ones, solutions, Eqs. (25a) and (25b), are favoured.

IV. DISCUSSIONS

We analyzed the solar, terrestrial and atmospheric neutrino experiments using the three-flavor neutrinos framework and got the allowed regions of the parameters (Δm_{12}^2 , $\sin^2 2\theta_{12}$, Δm_{23}^2 , θ_{13} , θ_{23}). In solar neutrino experiments, we got the large angle solution (Δm_{12}^2 , $\sin^2 2\theta_{12}$) = ($4 \times 10^{-6} - 7 \times 10^{-5} \text{eV}^2$, $0.6 - 0.9$) and small angle solution ($3 \times 10^{-6} - 1.2 \times 10^{-5} \text{eV}^2$, $0.003 - 0.01$) for $\theta_{13} = 0^\circ - 20^\circ$. When θ_{13} increases from 25° to 50° , large angle and small angle solutions merge. From the terrestrial and atmospheric neutrino experiments (not considering the zenith angle dependence), we got the allowed regions: ($\theta_{13} < 4^\circ$, $24^\circ < \theta_{23} < 26^\circ$) for large angle solution and $\Delta m_{23}^2 = 2 \text{eV}^2$, ($\theta_{13} < 4^\circ$, $24^\circ < \theta_{23} < 26^\circ$) and ($\theta_{13} < 2^\circ$, $64^\circ < \theta_{23} < 66^\circ$) for small angle solution and $\Delta m_{23}^2 = 2 \text{eV}^2$, ($\theta_{13} < 4^\circ$, $24^\circ < \theta_{23} < 62^\circ$) for large angle solution and $\Delta m_{23}^2 = 0.2 \text{eV}^2$, ($\theta_{13} < 4^\circ$, $24^\circ < \theta_{23} < 66^\circ$) for small angle solution and $\Delta m_{23}^2 = 0.2 \text{eV}^2$, ($\theta_{13} < 12^\circ$, $\theta_{23} \sim 40^\circ$, 48°) for large angle solution and $\Delta m_{23}^2 = 0.02 \text{eV}^2$, ($\theta_{13} < 14^\circ$, $\theta_{23} \sim 41^\circ$, 49°) for small angle solution and $\Delta m_{23}^2 = 0.02 \text{eV}^2$. When the zenith angle dependences are considered, the allowed regions are restricted to ($\Delta m_{12}^2 = 4 \times 10^{-6} - 7 \times 10^{-5} \text{eV}^2$, $\sin^2 2\theta_{12} = 0.6 - 0.9$, $\theta_{13} < 4^\circ$, $24^\circ < \theta_{23} < 26^\circ$) for $\Delta m_{23}^2 = 2 \text{eV}^2$, ($\Delta m_{12}^2 = 4 \times 10^{-6} - 7 \times 10^{-5} \text{eV}^2$, $\sin^2 2\theta_{12} = 0.6 - 0.9$, $\theta_{13} < 4^\circ$, $24^\circ < \theta_{23} < 45^\circ$) for $\Delta m_{23}^2 = 0.2 \text{eV}^2$ and ($\Delta m_{12}^2 = 4 \times 10^{-6} - 7 \times 10^{-5} \text{eV}^2$, $\sin^2 2\theta_{12} = 0.6 - 0.9$, $\theta_{13} < 12^\circ$, $\theta_{23} \sim 40^\circ$) for $\Delta m_{23}^2 = 0.02 \text{eV}^2$. If we include LSND experiment in terrestrial experiments, allowed regions are restricted to ($\Delta m_{12}^2 = 4 \times 10^{-6} - 7 \times 10^{-5} \text{eV}^2$, $\sin^2 2\theta_{12} = 0.6 - 0.9$, $2^\circ < \theta_{13} < 4^\circ$, $24^\circ < \theta_{23} < 26^\circ$) and $\Delta m_{23}^2 = 2 - 0.2 \text{eV}^2$.

Finally, we present the neutrino mixing matrix Eq. (2) numerically for the allowed solutions Eqs. (25a), (25b) and (25c);

$$\text{for } \Delta m_{23}^2 = 2 \text{eV}^2$$

$$U = \begin{pmatrix} 0.81 \leftrightarrow 0.90 & 0.43 \leftrightarrow 0.58 & 0.0 \leftrightarrow 0.07 \\ -0.39 \leftrightarrow -0.56 & 0.71 \leftrightarrow 0.83 & 0.41 \leftrightarrow 0.44 \\ 0.12 \leftrightarrow 0.26 & -0.33 \leftrightarrow -0.42 & 0.90 \leftrightarrow 0.91 \end{pmatrix}, \quad (26a)$$

$$\text{for } \Delta m_{23}^2 = 0.2 \text{eV}^2$$

$$U = \begin{pmatrix} 0.81 \leftrightarrow 0.90 & 0.43 \leftrightarrow 0.58 & 0.0 \leftrightarrow 0.07 \\ -0.30 \leftrightarrow -0.56 & 0.54 \leftrightarrow 0.83 & 0.41 \leftrightarrow 0.71 \\ 0.12 \leftrightarrow 0.41 & -0.33 \leftrightarrow -0.64 & 0.71 \leftrightarrow 0.91 \end{pmatrix}, \quad (26b)$$

for $\Delta m_{23}^2 = 0.02 \text{ eV}^2$

$$U = \begin{pmatrix} 0.79 \leftrightarrow 0.90 & 0.42 \leftrightarrow 0.58 & 0.0 \leftrightarrow 0.24 \\ -0.33 \leftrightarrow -0.57 & 0.53 \leftrightarrow 0.69 & 0.62 \leftrightarrow 0.64 \\ 0.11 \leftrightarrow 0.38 & -0.52 \leftrightarrow -0.66 & 0.74 \leftrightarrow 0.77 \end{pmatrix}. \quad (26c)$$

APPENDIX A: NUMERICAL ANALYSIS FOR R IN SOLAR NEUTRINO

The ratio R of the detected e neutrino flux to the expected e neutrino flux deduced from SSM is expressed as

$$R = \frac{\int_{E_{min}}^{E_{max}} P_{3\nu}^{\text{MSW}}(E) f(E) dE}{\int_{E_{min}}^{E_{max}} f(E) dE}, \quad (A1)$$

where E is the neutrino energy and $f(E)$ is the summation of products of $f_i(E)$ and c_i^D .

$$f(E) = \sum_i c_i^D f_i(E). \quad (A2)$$

$f_i(E)$ represents the neutrino flux produced in the reaction of type i , where $i = pp, {}^{13}\text{N}, {}^{15}\text{O}, {}^7\text{Be}, {}^8\text{B}$ and pep , at the center of the sun. c_i^D is the detector sensitivity of detector D for the neutrino flux of type i . From the SSM [23,28], neutrino fluxes at 1AU are expressed as the function of E (numerical number without dimension of neutrino energy measured in the unit MeV) as

$$f_{pp}(E) = E^{1.88}(4.358 - 0.0946E - 24.48E^2) \times 10^{12}, \quad (E < 0.420 \text{ MeV}) \quad (A3a)$$

$$f_{Be1}(E) = 8 \times 10^8, \quad (0.384 - 0.25 \text{ MeV} < E < 0.384 + 0.25 \text{ MeV}) \quad (A3b)$$

$$f_N(E) = E^{1.88}(4.194 - 4.541E + 0.870E^2) \times 10^9, \quad (E < 1.199 \text{ MeV}) \quad (A3c)$$

$$f_{Be2}(E) = 4 \times 10^9, \quad (0.862 - 0.5 \text{ MeV} < E < 0.862 + 0.5 \text{ MeV}) \quad (A3d)$$

$$f_O(E) = E^{1.88}(12.74 - 7.919E + 0.328E^2) \times 10^8, \quad (E < 1.732 \text{ MeV}) \quad (A3e)$$

$$f_{pep}(E) = 1.5 \times 10^8, \quad (1.442 - 0.5 \text{ MeV} < E < 1.442 + 0.5 \text{ MeV}) \quad (A3f)$$

$$f_B(E) = E^{1.88}(81211 - 11500E - 407.1E^2). \quad (E < 14.02 \text{ MeV}) \quad (A3g)$$

We estimate the detector sensitivity which is normalized as $c_B^D = 1$ using the Bahcall's result (Table I) [23],

$$\text{Ga experiment : } c_{pp}^{Ga} = 9.62 \times 10^{-4}, c_N^{Ga} = 2.73 \times 10^{-3}, c_{Be1,Be2}^{Ga} = 3.61 \times 10^{-3}, \\ c_O^{Ga} = 4.30 \times 10^{-3}, c_{pep}^{Ga} = 8.93 \times 10^{-3}, c_B^{Ga} = 1.0, \quad (\text{A4a})$$

$$\text{Cl experiment : } c_{pp}^{Cl} = 0, c_N^{Cl} = 4.82 \times 10^{-4}, c_{Be1}^{Cl} = 0, c_{Be2}^{Cl} = 5.08 \times 10^{-4}, \\ c_O^{Cl} = 7.64 \times 10^{-4}, c_{pep}^{Cl} = 1.44 \times 10^{-3}, c_B^{Cl} = 1.0, \quad (\text{A4b})$$

$$\text{Kamiokande experiment : } c_{pp}^{Kam} = 0, c_N^{Kam} = 0, c_{Be1}^{Kam} = 0, c_{Be2}^{Kam} = 0, c_O^{Kam} = 0, \\ c_{pep}^{Kam} = 0, c_B^{Kam} = 1.0. \quad (\text{A4c})$$

Numerical values used for parameters at the center of the sun are as follows:

$$A = 2\sqrt{2}G_F N_e E = 2\sqrt{2}G_F (Y_e/m_n)\rho E, \quad (\text{A5a})$$

$$G_F = 1.17 \times 10^{-23} \text{eV}^{-2} \text{ (Fermi constant),}$$

$$Y_e = 1/2 \text{ (the number of electrons per nucleon),}$$

$$m_n = 939 \text{ MeV} \text{ (the nucleon mass), } \rho = 156 \text{ g/cm}^3 \text{ (the density),}$$

$$\left| \frac{1}{N_e} \frac{dN_e}{dx} \right|_0 = 2.91 \times 10^{-15}. \quad (\text{A5b})$$

APPENDIX B: EXPLICIT E_α DEPENDENCE OF $f_\alpha(E_\alpha, \theta_\alpha)$

We take the E_α dependence of $f_\alpha(E_\alpha, \theta_\alpha)$ from the results estimated in Monte Carlo calculation. We neglect the θ_α dependence of $f_\alpha(E_\alpha, \theta_\alpha)$. For the sub-Gev experiments, we take it from Ref. [6] as

$$f_{\nu_\mu}(E, \theta) = N_s(-2.89E^{-2.55} + 22.9E^{-1.55} - 12.7E^{-0.55}), \quad (\text{B1a})$$

$$f_{\nu_e}(E, \theta) = N_s(-1.18E^{-2.55} + 9.98E^{-1.55} - 3.90E^{-0.55}), \quad (\text{B1b})$$

and for the multi-GeV experiments from Ref. [7] as

$$f_{\nu_\mu}(E, \theta) = N_m(42.1 - 383E^{-2} + 374E^{-1} - 2.42E + 0.0403E^2 \quad (\text{B2a})$$

$$-0.000206E^3), \text{ fully-and partially-contained events} \quad (\text{B2b})$$

$$f_{\nu_e}(E, \theta) = N_m(-9.54 - 225E^{-2} + 249E^{-1} + 0.156E - 0.000658E^2 \quad (\text{B2c})$$

$$-2.42 \times 10^{-6}E^3), \text{ fully-contained events} \quad (\text{B2d})$$

where E is the numerical number of neutrino energy measured in unit GeV, and N_s and N_m are constants with the unit: number of events/GeV.

REFERENCES

- [1] S. L. Glashow, Nucl. Phys. **22**, 579(1961). S. Weinberg, Phys. Rev. Lett. **19**, 1264(1967). A. Salam, in Elementary Particle Theory, ed. N. Svartholm (Almqvist and Wiksell, Stockholm, 1968) p.367.
- [2] SAGE Collaboration, J. N. Abdurashitov *et al.*, Phys. Lett. **B328**, 234(1994).
- [3] GALLEX Collaboration, P. Anselmann *et al.*, Phys. Lett. **B357**, 237(1995).
- [4] B. T. Cleveland *et al.*, Nucl. Phys. **B**(Proc. Suppl.)**38**, 47(1995).
- [5] Kamiokande Collaboration, K. S. Hirata *et al.*, Phys. Rev. **D44**, 2241(1991); Phys. Rev. Lett. **66**, 9(1991).
- [6] Kamiokande Collaboration, K. S. Hirata *et al.*, Phys. Lett. **B280**, 146(1992).
- [7] Kamiokande Collaboration, Y. Fukuda *et al.*, Phys. Lett. **B335**, 237(1994).
- [8] IMB Collaboration, R. Becker-Szendy *et al.*, Phys. Rev. **D46**, 3720(1992).
- [9] J. R. Primack, J. Holtzman, A. Klypin and D. O. Caldwell, Phys. Rev. Lett. **74**, 2160(1995). D. N. Schramm, Nucl. Phys. **B**(Proc. Suppl.)**38**, 349(1995).
- [10] E531 Collaboration, N. Ushida *et al.*, Phys. Rev. Lett. **57**, 2897(1986).
- [11] K. Winter, Nucl. Phys. **B**(Proc. Suppl.)**38**, 211(1995).
- [12] E776 Collaboration, L. Borodovsky *et al.*, Phys. Rev. Lett. **68**, 274(1992).
- [13] KARMEN Collaboration, B. Armbruster *et al.*, Nucl. Phys. **B**(Proc. Suppl.)**38**, 235(1995).
- [14] LSND Collaboration, C. Athanassopoulos *et al.*, Phys. Rev. Lett. **75**, 2650 (1995). J. E. Hill, Phys. Rev. Lett. **75**, 2654(1995). W. C. Louis, Nucl. Phys. **B**(Proc. Suppl.)**38**, 229(1995).
- [15] B. Achkar *et al.*, Nucl. Phys. **B434**, 503(1995).
- [16] S. P. Mikheyev and A. Yu. Smirnov, Phys. Lett. **B200**, 560(1988). K. Hidaka, M. Honda and S. Midorikawa, Phys. Rev. Lett. **61**, 1537(1988).
- [17] T. Kuo and J. Pantaleone, Rev. Mod. Phys. **61**, 937(1989).
- [18] G. L. Fogli, E. Lisi and D. Montanino, Phys. Rev. **D52**, 2775(1995). G. L. Fogli, E. Lisi and D. Montanino, Phys. Rev. **D54**, 2048(1996).
- [19] Y. Totsuka(SuperKamiokande Collaboration), in *LP'97*, 28th International Symposium on Lepton Photon Interactions, Hamburg, Germany, 1997, to appear in the Proceedings.

- [20] K. Kaneyuki(SuperKamiokande Collaboration), in *1997 Sectional Meetings of the Physical Society of Japan*, Tokyo Metropolitan Univ., Japan, 1997.
- [21] Y. Suzuki, in *Proceedings of 28th International Conference on High Energy Physics*, Warsaw, Poland, 1996, eddited by Z. Ajduk and A. K. Wroblewski (Warsaw University), p.273.
- [22] L. Wolfenstein, Phys. Rev. **D17**, 2369(1978). S. P. Mikheev and A. Yu. Smirnov, Sov. J. Nucl. Phys. **42**(6), 913(1985).
- [23] J. N. Bahcall and M. H. Pinsonneault, Rev. Mod. Phys. **67**, 781(1995).
- [24] S. A. Bludman, N. Hata, D. C. Kennedy, and P. G. Langacker, Phys. Rev. **D47**, 2220(1993). N. Hata and P. Langacker, Phys. Rev. **D50**, 632(1994).
- [25] T. K. Gaisser, T. Stanev and G. Barr, Phys. Rev. **D38**, 85(1988).
- [26] M. Honda *et al.*, Phys. Rev. **D52**, 4985(1995).
- [27] Vivek Agrawal *et al.*, Phys. Rev. **D53**, 1314(1996).
- [28] Particle Data Group, Phys. Rev. **D54**, 1(1996).

FIGURES

FIG. 1. Contour plot of R for $\theta_{13} = 0$ on $\sin^2 2\theta_{12} - \Delta m_{12}^2$ plane. Each two contours denoted as Ga, Cl and Kam corresponds to the upper and lower value of R for Ga, Cl and Kamiokande experiment, respectively. Two solutions are denoted as common areas enclosed by each two contours of Ga, Cl and Kam.

FIG. 2. The plots of allowed regions of the combined Ga, Cl and Kam experiments using the χ -square, where the solid thin, solid thick and dotted lines define the regions allowed at 99%, 95% and 90% C.L., respectively. Figs. (a) - (h) show the allowed regions for $\theta_{13} = 0^\circ - 50^\circ$.

FIG. 3. The plots of allowed regions on $\theta_{13} - \theta_{23}$ plane determined by P of terrestrial $\nu_\mu \rightarrow \nu_\tau$, $\nu_\mu \rightarrow \nu_e$, $\bar{\nu}_\mu \rightarrow \bar{\nu}_e$ and $\bar{\nu}_e \rightarrow \bar{\nu}_e$ experiments. Allowed regions are corners, left and right hand sides surrounded by curves. Curves represent the boundary of 90 % C.L. of P . Δm_{12}^2 and $\sin^2 2\theta_{12}$ are fixed as 10^{-5}eV^2 and 0.8, respectively. Δm_{23}^2 is fixed to 20eV^2 (Fig. 3(a)), 2.0eV^2 (Fig. 3(b)), 0.2eV^2 (Fig. (c)) and 0.02eV^2 (Fig. (d)). Dotted lines show the allowed regions restricted by the LSND data.

FIG. 4. The plots of allowed regions of $R(\mu/e)$ of atmospheric neutrinos for various values of Δm_{23}^2 on $\tan^2 \theta_{13} - \tan^2 \theta_{23}$. Figs. (a)-(d) show the plots of sub-GeV experiments and Figs. (e)-(h) the ones of multi-GeV experiments. We fix the parameters $(\Delta m_{12}^2, \sin^2 2\theta)$ to be $(3 \times 10^{-5}\text{eV}^2, 0.7)$ corresponding to the large angle solution (solid lines) and $(10^{-5}\text{eV}^2, 0.005)$ corresponding to the small angle solution (dotted lines).

FIG. 5. The zenith angle dependence of $R(\mu/e)$ in atmospheric neutrino experiment. Experimental data is referred to Ref. [20]. Fig. (a) represents the sub-GeV experimental case: solid curve is given on a typical parameters for large angle solution ($\Delta m_{12}^2 = 3 \times 10^{-5}\text{eV}^2$, $\sin^2 2\theta_{12} = 0.7$, $\Delta m_{23} = 0.2\text{eV}^2$, $\theta_{13} = 4^\circ$, $\theta_{23} = 25^\circ$) and dotted curve on small angle solution ($\Delta m_{12}^2 = 10^{-5}\text{eV}^2$, $\sin^2 2\theta_{12} = 0.007$, $\Delta m_{23} = 0.2\text{eV}^2$, $\theta_{13} = 4^\circ$, $\theta_{23} = 25^\circ$). Fig. (b) represents the multi-GeV experimental case: solid curve is given on parameters for large angle solution ($\theta_{13} = 4^\circ$, $\theta_{23} = 30^\circ$) and dotted curve on small angle solution ($\theta_{13} = 4^\circ$, $\theta_{23} = 30^\circ$).

TABLES

TABLE I. Individual neutrino contribution (averaged on the cases with and without diffusion) calculated by Bahcall(1995)

| neutrino source | Cl(SNU) | Ga(SNU) |
|-----------------|---------|---------|
| <i>pp</i> | 0.00 | 70 |
| <i>pep</i> | 0.23 | 3 |
| ^{7}Be | 1.17 | 35 |
| ^{8}B | 6.4 | 14 |
| ^{13}N | 0.09 | 3 |
| ^{15}O | 0.3 | 5 |
| total | 8.2 | 132 |

TABLE II. The results of atmospheric experiments predicting the anomaly. Sub-GeV experiments detect the visible-energy less than 1.33GeV, and in the second column (total exposure), left number represents the detector exposure in which fully contained events are detected and right numbers partially contained events.

| Experiments | Total exposure(ktyr) | $R(\mu/e)$ (double ratio) |
|---------------------------------|----------------------|---------------------------------|
| Kamiokande(sub-Gev) [6] | 4.92 | $0.60^{+0.07}_{-0.06} \pm 0.05$ |
| Kamiokande(multi-GeV) [7] | 8.2, 6.0 | $0.57^{+0.08}_{-0.07} \pm 0.07$ |
| IMB [8] | 7.7 | $0.54 \pm 0.02 \pm 0.07$ |
| SuperKamiokande(sub-GeV) [20] | 20, 18 | $0.63 \pm 0.03 \pm 0.05$ |
| SuperKamiokande(multi-GeV) [20] | 20, 18 | $0.60 \pm 0.06 \pm 0.07$ |

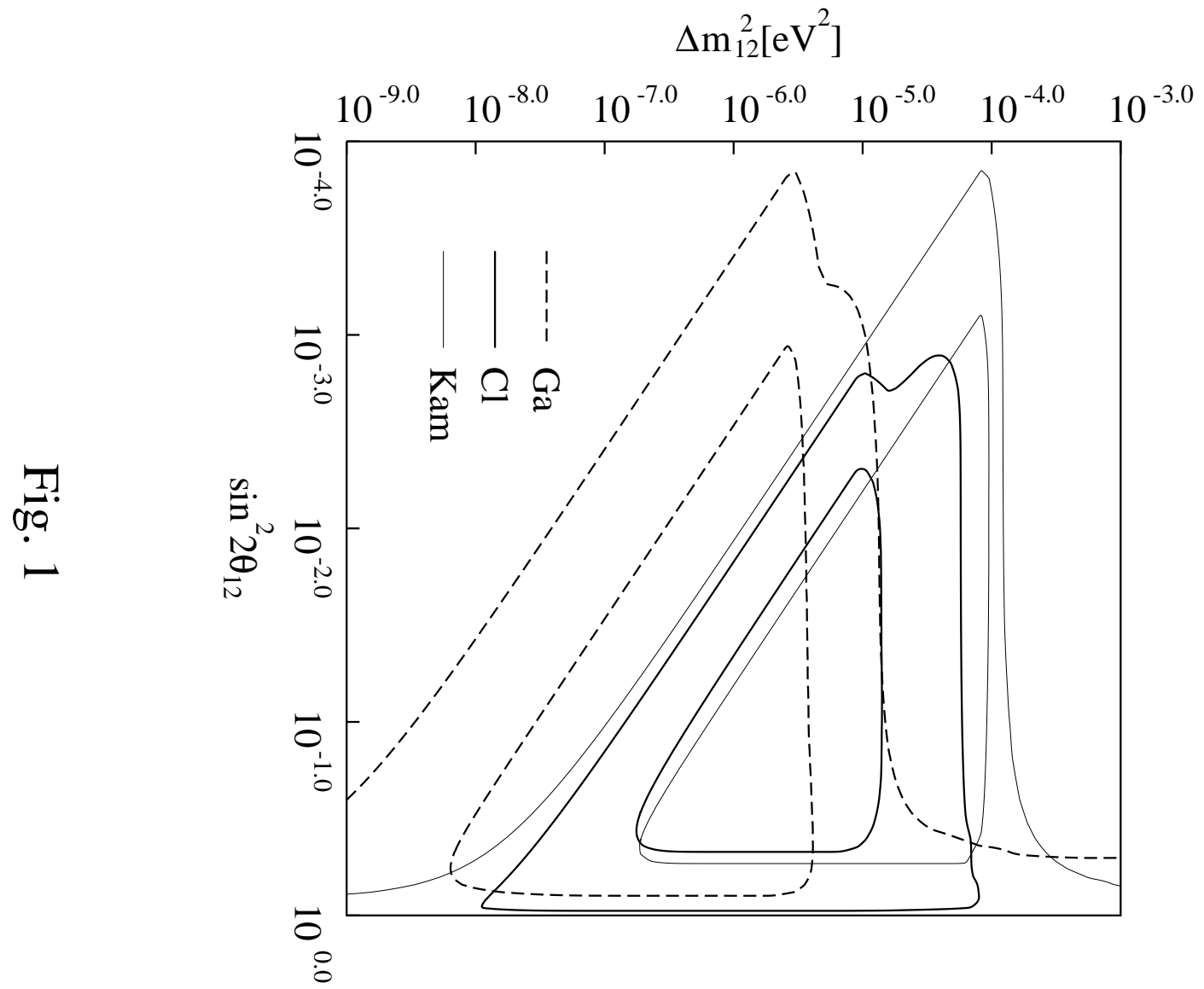


Fig. 1

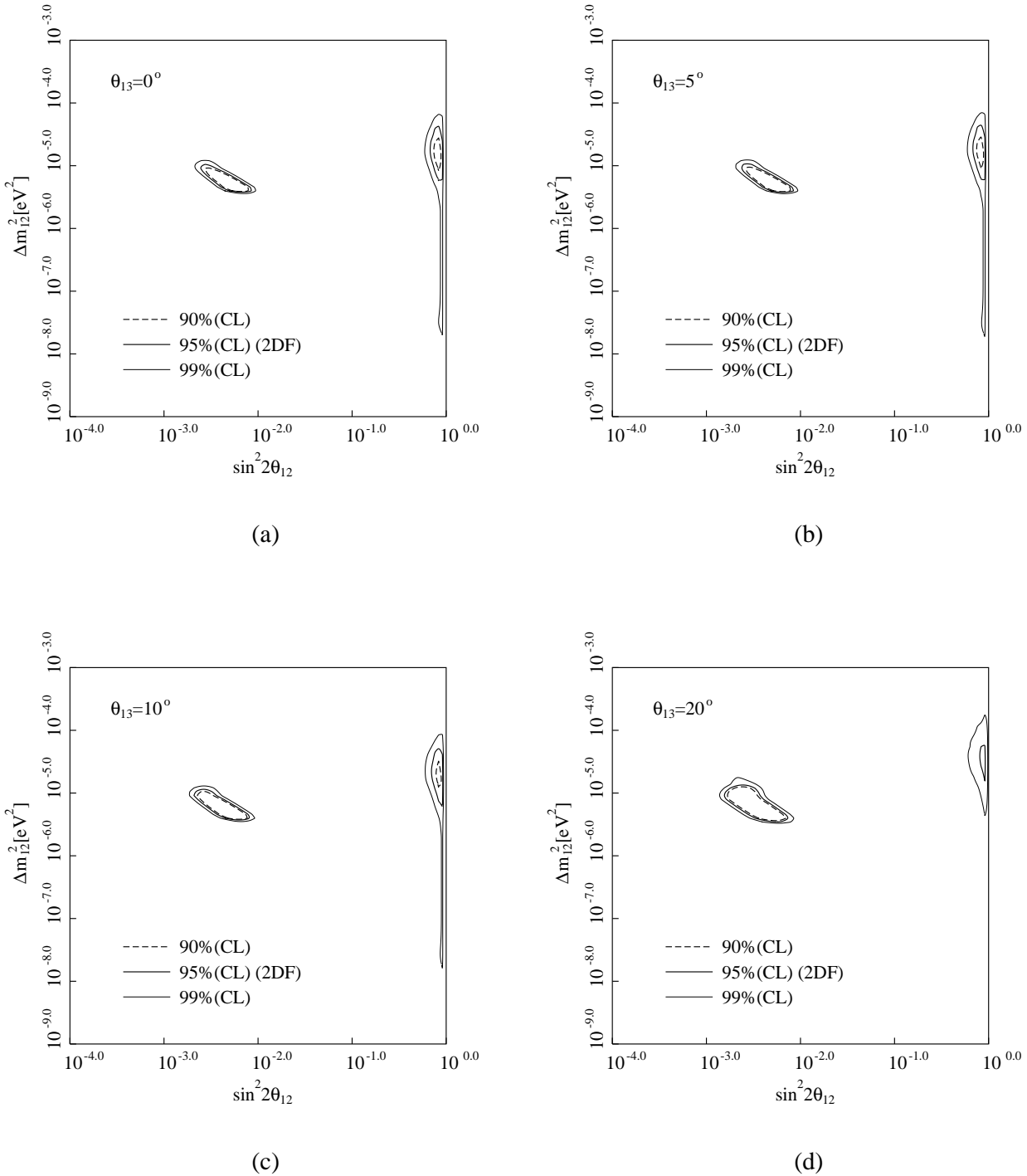
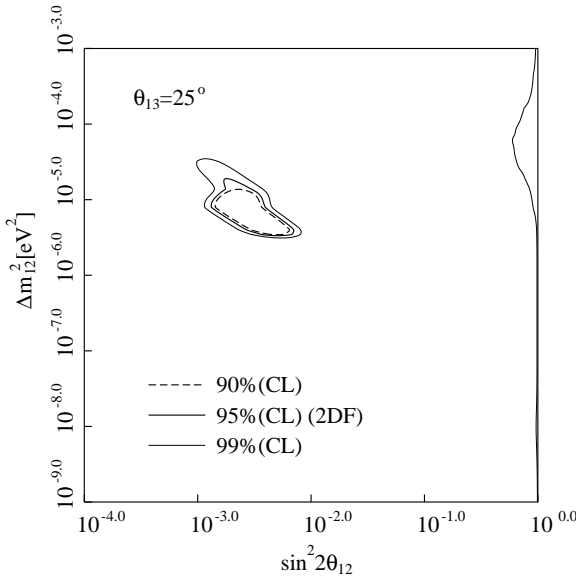
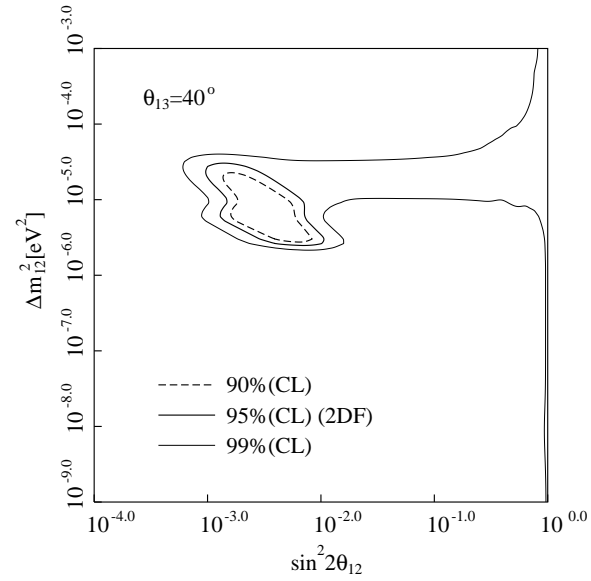


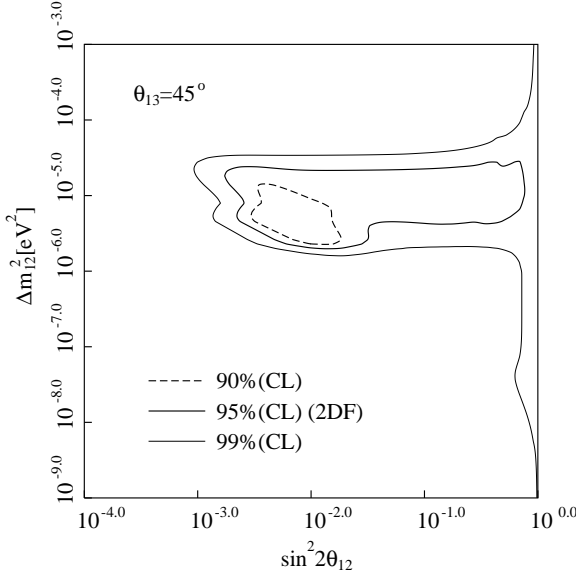
Fig. 2



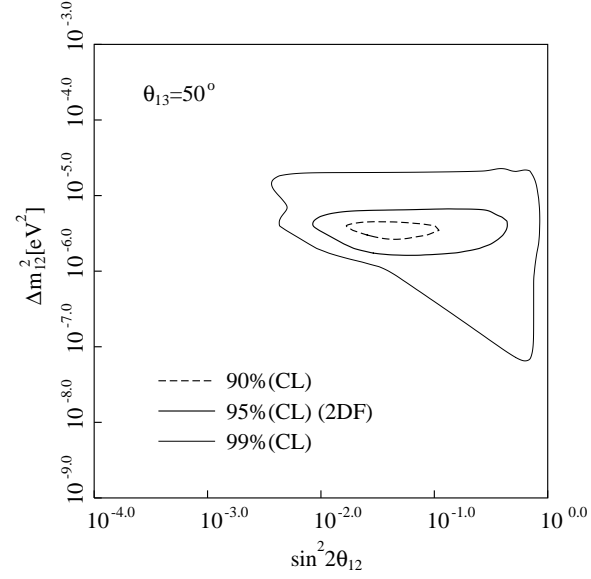
(e)



(f)

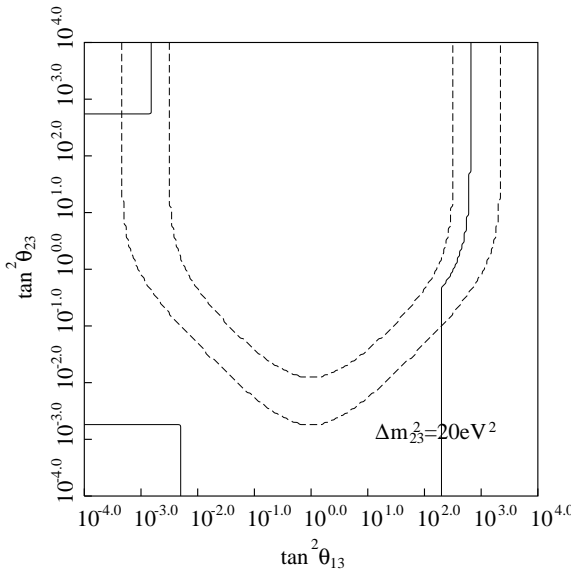


(g)

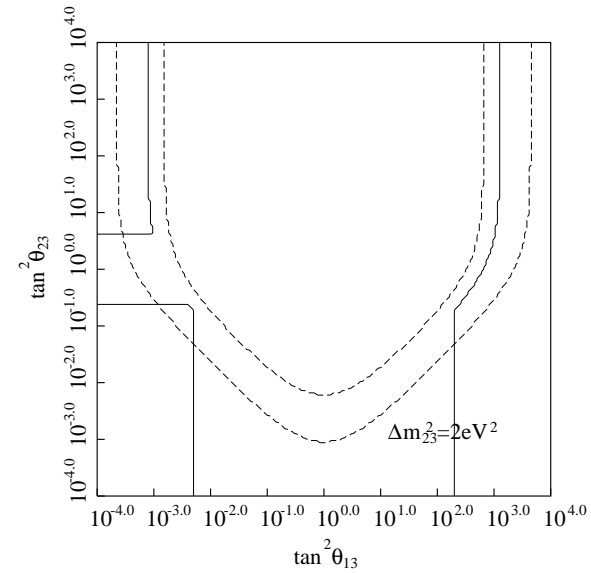


(h)

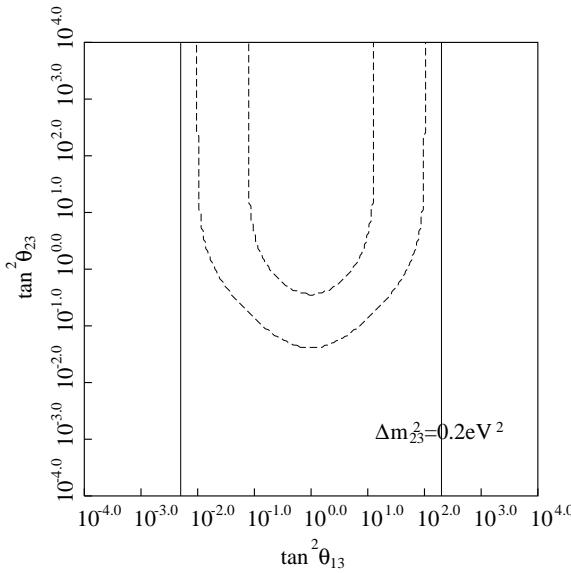
Fig. 2



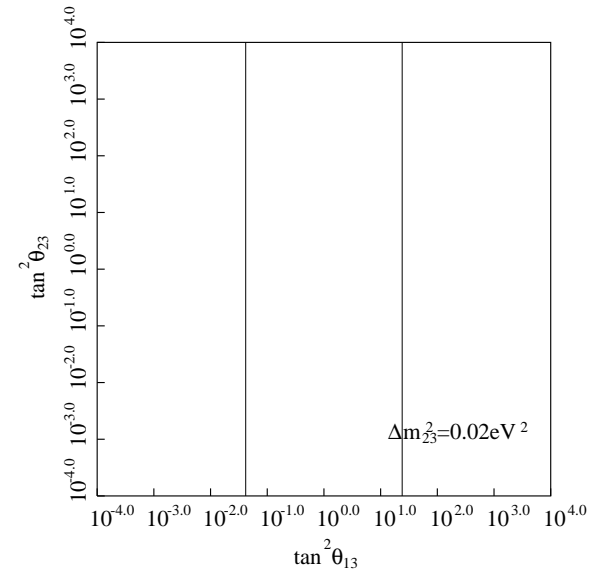
(a)



(b)

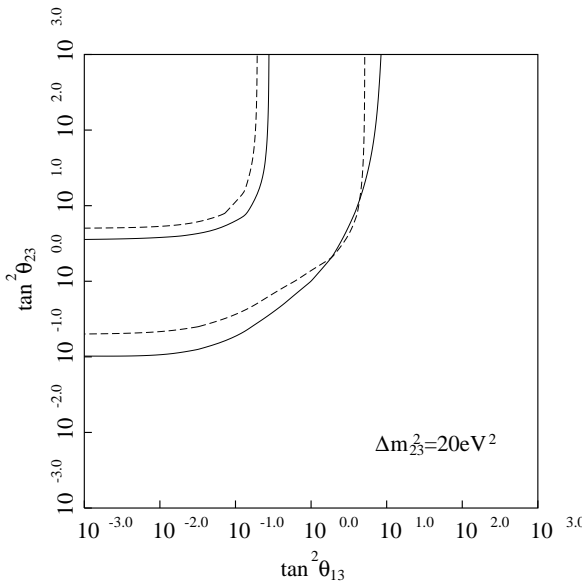


(c)

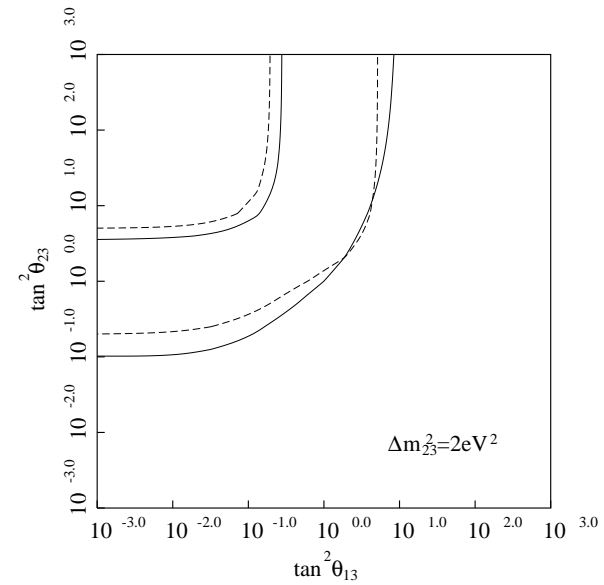


(d)

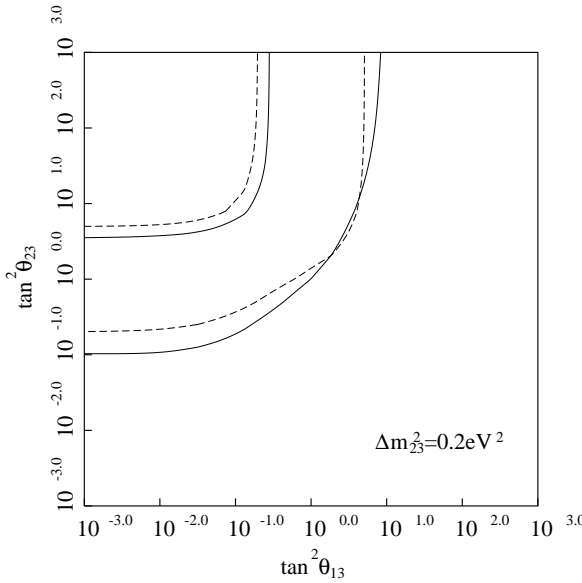
Fig. 3



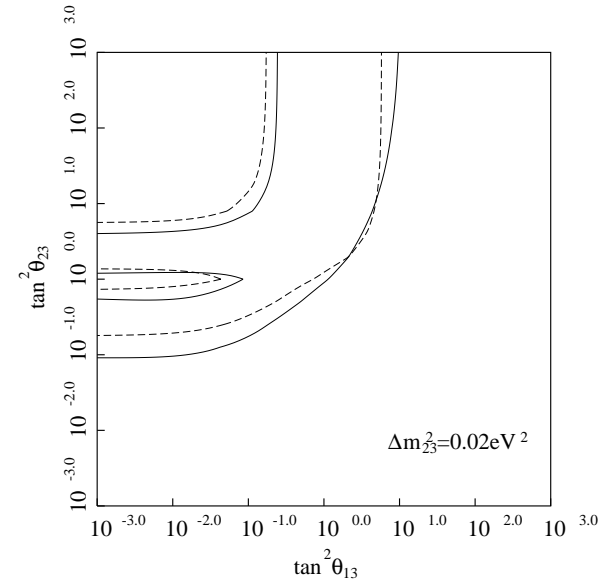
(a)



(b)

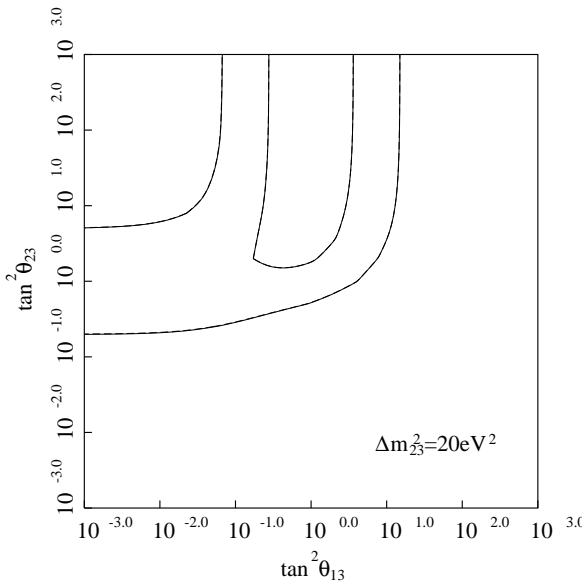


(c)

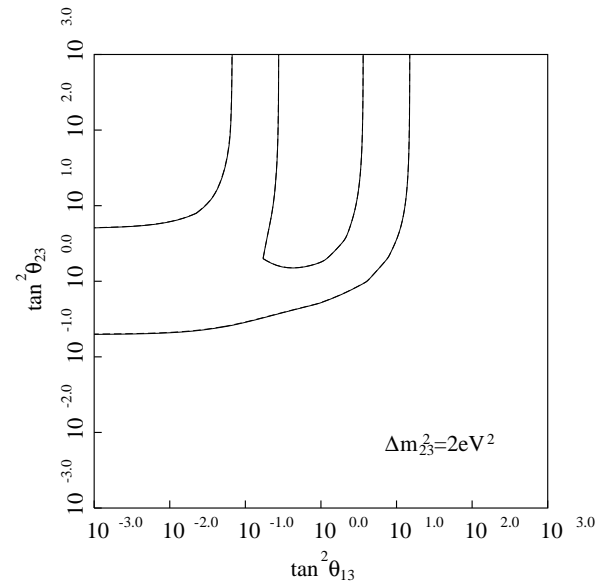


(d)

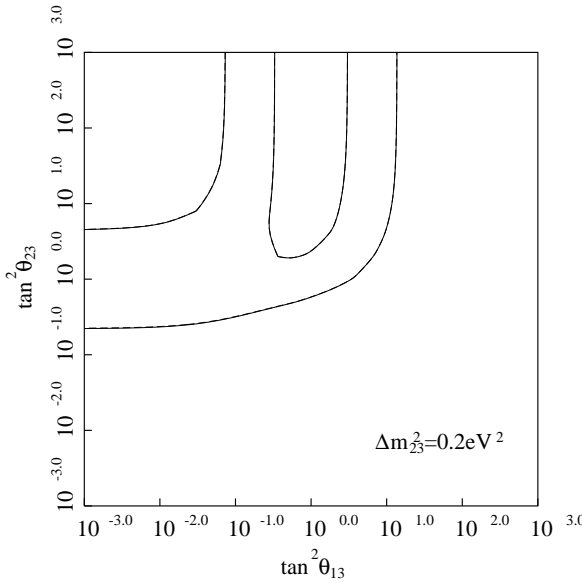
Fig. 4



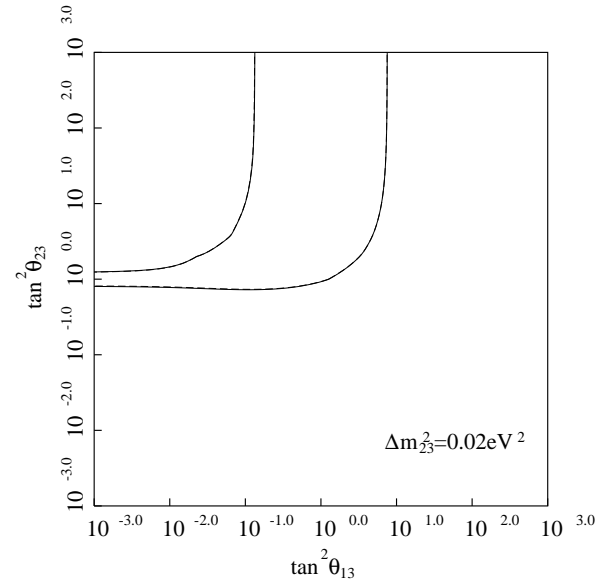
(e)



(f)



(g)



(h)

Fig. 4

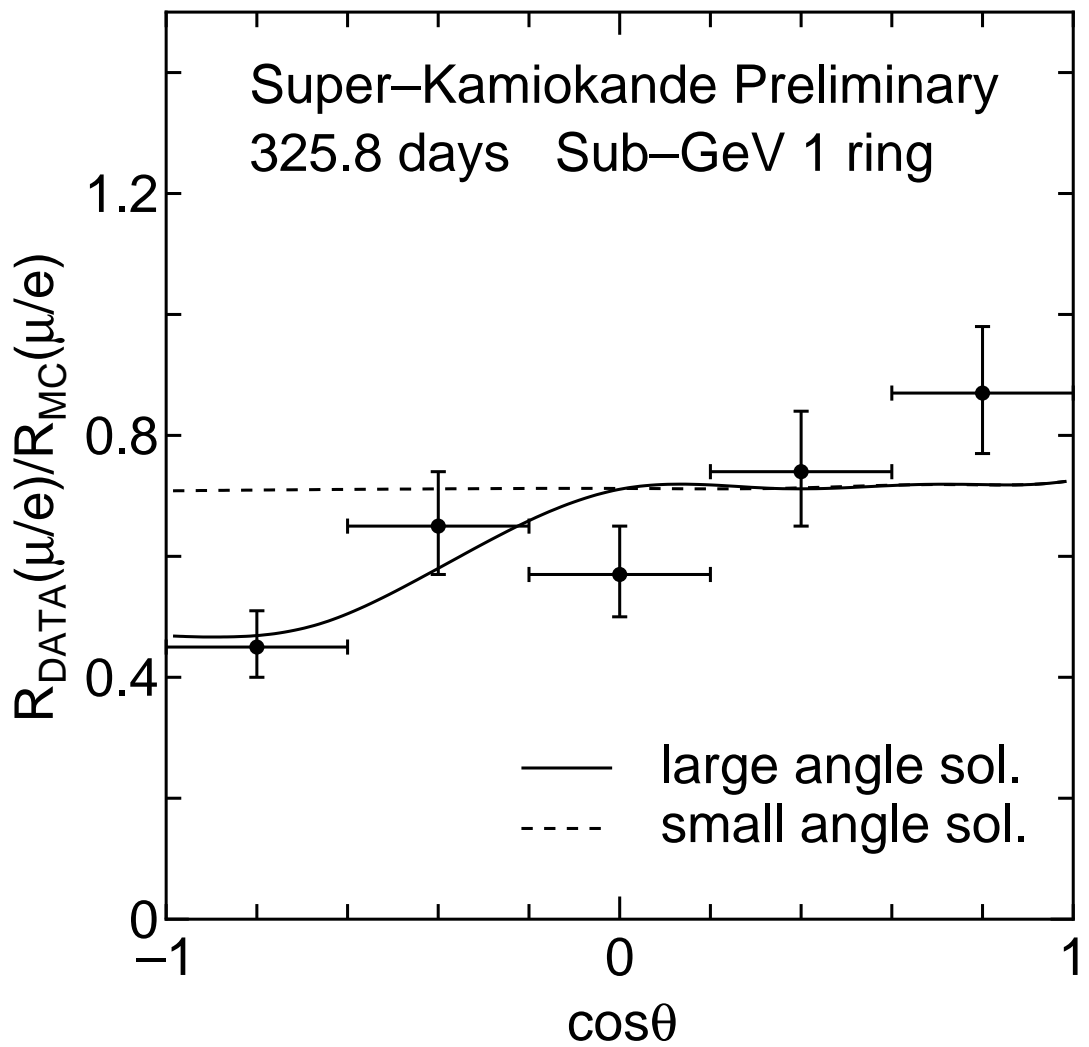


Fig. 5(a)

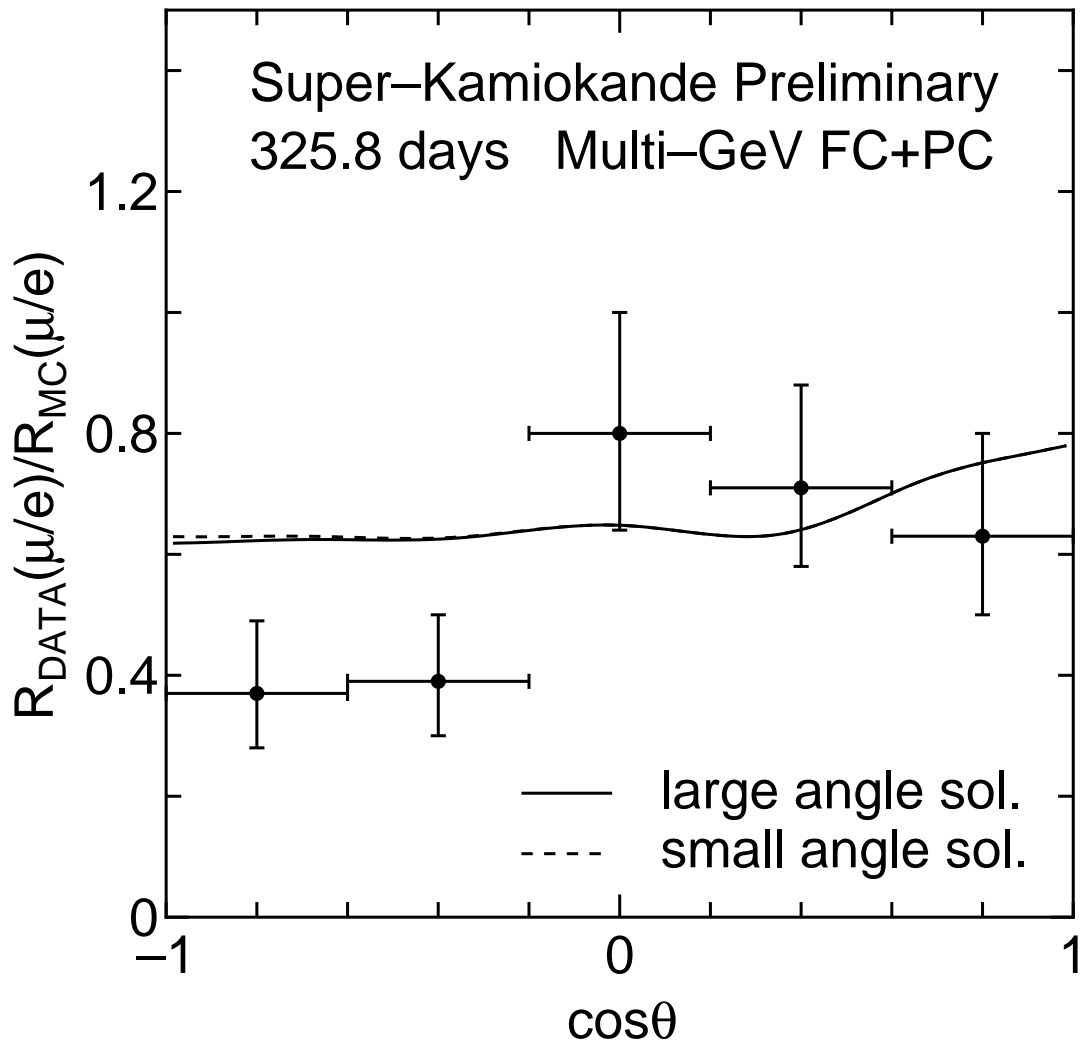


Fig. 5(b)